AIAA JOURNAL
Vol. 32, No. 3, March 1994

Development of a Large-Aspect-Ratio Rectangular Turbulent Free Jet

W. R. Quinn*
St. Francis Xavier University, Antigonish, Nova Scotia B2G 1C0, Canada

This paper reports the results of detailed mean flow and turbulence measurements made with hot-wire anemometry in the flowfield of a turbulent free jet of air issuing from a sharp-edged rectangular slot of aspect ratio 20 into still air surroundings. All three components of the mean velocity vector, the three Reynolds normal stresses and the two Reynolds primary shear stresses were measured. The mean streamwise vorticity and the turbulence kinetic energy have been calculated from the relevant measured data. It was found that the cross section of the jet, in the near flowfield, is dominated by counter-rotating streamwise vortices that facilitate rapid near-field mixing. Rapid mixing is also evidenced by a short potential core length and high values of the turbulence kinetic energy and the Reynolds primary shear stresses compared with those found in an axisymmetric jet at the corresponding streamwise locations. In addition, mean streamwise velocity off-center peaks, which may be the result of the self-induction of the counter-rotating streamwise vortices, were found in the near flowfield, and the jet was found to spread monotonically in the central plane of the slot minor axis and to contract initially in the central plane of the slot major axis.

Nomenclature

A, B	= constants in hot-wire exponent power law
$Bhlf$	= general jet half-velocity width
C_u	= kinematic virtual origin
D_e	= equivalent diameter
E	= hot-wire output voltage
K_u	= mean streamwise velocity decay rate
n	= exponent in hot-wire exponent power law
Q_s	= secondary flow velocity vector, $[\sqrt{\overline{V^2}+\overline{W^2}}]$
q^2	= turbulence kinetic energy, $[(\overline{u'^2}+\overline{v'^2}+\overline{w'^2})/2]$
U	= mean streamwise velocity
U_{eff}	= effective hot-wire cooling velocity
$\overline{u'^2}$	= streamwise Reynolds normal stress
$\overline{u'v'}$	= spanwise Reynolds primary shear stress
$\overline{u'w'}$	= lateral Reynolds primary shear stress
V	= mean spanwise velocity
$\overline{v'^2}$	= spanwise Reynolds normal stress
$\overline{v'w'}$	= Reynolds secondary shear stress
W	= mean lateral velocity
$\overline{w'^2}$	= lateral Reynolds normal stress
X	= streamwise coordinate
Y	= spanwise coordinate
$Yhlf$	= jet half-velocity width in the Y direction
Z	= lateral coordinate
$Zhlf$	= jet half-velocity width in the Z direction
ν	= kinematic viscosity
Ω_x	= mean streamwise vorticity, $(\partial W/\partial Y - \partial V/\partial Z)$
Ω_y	= mean spanwise vorticity
Ω_z	= mean lateral vorticity
∇^2	= Laplace operator

Subscripts

cl	= centerline value
max	= maximum value on the jet centerline

Received Feb. 17, 1993; revision received Aug. 28, 1993; accepted for publication Aug. 30, 1993.

*Associate Professor, Department of Engineering. Member AIAA.

Introduction

RECTANGULAR jets are utilized in diverse technical areas. In aerospace engineering, for example, these jets are used in propulsion units and in lift-producing devices. Manufacturing and economic expediency often dictate that the jets issue from slots, with sharp edges, cut in flat surfaces.

Many studies involving turbulent free jets issuing from sharp-edged rectangular slots have appeared in the literature.[1-10] However, a study reporting detailed measurements, made in the entire plane of the cross section of a large-aspect-ratio rectangular jet at several streamwise locations, is not yet available. Such a study is needed to shed some light on the mixing process (i.e., momentum transfer) in turbulent free rectangular jets. It should be noted[10] that the speed of mixing in these jets increases with increase in the slot aspect ratio as long as the flow remains three dimensional.

The present experimental study of a turbulent free jet issuing from a sharp-edged rectangular slot of aspect ratio 20 was done to satisfy the previously mentioned need. Detailed measurements of the time-averaged mean flow and turbulence quantities, which were made with hot-wire anemometry in the entire plane of the jet cross section at several streamwise locations, are used to show the development of the jet downstream of the slot exit plane and to shed some light on the near-field mixing process. The data can also be used to facilitate turbulence modeling of three-dimensional flows. The exit plane Reynolds number, based on the equivalent diameter (D_e = 0.0453 m), which is the same as the diameter of a round slot with the same exit area as the rectangular slot, was about 2.08×10^5. The mean streamwise velocity and streamwise turbulence intensity at the center of the slot exit plane were 60 m/s and 0.5%, respectively.

Experimental Details

The jet flow facility used in the present study is the open-loop, blower type, and it has been described in detail elsewhere.[11] A sketch of the flow facility is shown in Fig. 1a along with the coordinate system that is used in this study. The Z coordinate, which is perpendicular to the plane in which X and Y lie and forms a right-hand system with them, is not shown in Fig. 1a. The flow facility consists of a centrifugal fan, a $0.76 \times 0.76 \times 1.23$ m plywood box, which serves as a settling chamber, fitted with honeycomb and mesh wire screens, a three-dimensional contraction whose contour is based on a third-degree polynomial with zero first derivatives as end conditions, and the sharp-edged rectangular slot of aspect ratio 20. The slot was assembled in a 0.305×0.305-m retaining plate

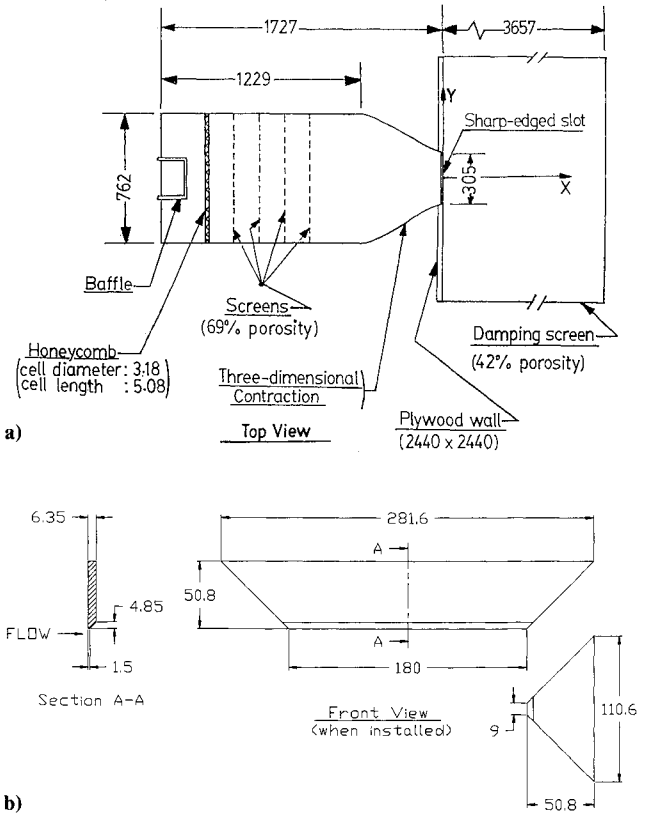

Fig. 1 Sketch of the flow facility and slot detail. All dimensions are in millimeters.

from four machine-mitred pieces of aluminum in accordance with the specifications of British Standard 1042 (1973), and the retaining plate was attached to the downstream end of the contraction. Two of the machine-mitred pieces of aluminum are shown in Fig. 1b. The jet issues into a cage that extends 3.66 m downstream and is covered on the top and sides with steel damping screens of 42% porosity. The screens help to minimize the effect of room draughts generated by the jet blowing into a room of finite size (7.70 × 7.01 × 2.87 m). The upstream end of the cage was flush with a 2.44 × 2.44 m plywood wall, and the downstream end was open.

The movement of the sensing probe in the flowfield was facilitated by a three-dimensional traversing system that was driven by stepping motors under microcomputer control. The sensing probe could be positioned to within 0.3 mm in the streamwise direction and to within 0.01 mm in the spanwise and lateral directions. The traversing system employed a rack and pinion system in the streamwise direction and lead screws in the spanwise and lateral directions.

Dantec x-array hot-wire probes (55P61) were utilized for the measurement of the mean and fluctuating velocities. The hot-wire probes, which were operated by constant temperature anemometers at a resistance ratio of 1.8, were calibrated on line on the jet centerline in the very near flowfield against the output of a pitot-static tube that was connected to a pressure transducer and a Barocel electronic manometer. The calibration data were fitted to the exponent power law: $E^2 = A + BU_{\text{eff}}^n$, and A, B, and n were optimized with a linear least-squares goodness-of-fit procedure. A "cosine law" response to yaw was assumed, and the effective angle was found from a yaw calibration following Bradshaw.[12] The hot-wire signals were linearized by the laboratory microcomputer and digitized, at about 1 kHz, by a 12-bit successive approximation A/D converter. A two-channel sample-and-hold unit with very low droop rate, two low-pass analog filters, and amplifiers were used for signal processing and signal conditioning. The data reduction was performed in real time using the laboratory microcomputer. Temperature variations from the calibration temperature were monitored with a thermocouple placed in close proximity to the hot-wire probe, and corrections for such variations were made, using the procedure in Bearman[13] in the data-reduction software. The correction formulas proposed by Champagne and Sleicher,[14] for the effect of tangential cooling of x-array hot-wire probes, were also incorporated in the data-reduction software.

Results and Discussion

The decay of the mean streamwise velocity along the jet centerline is shown in Fig. 2 along with the results of Sforza et al.[15] and Sfeir.[2] Note that the maximum mean streamwise velocity on the jet centerline is found, because of the existence of a vena contracta in jets issuing from sharp-edged slots, downstream of the slot exit plane. A very short constant mean streamwise velocity region (0.50 D_e in length), representing the potential core, is followed by a nonlinear decay region in the near flowfield and a linear decay region in the far flowfield. The very short potential core length implies, as has been shown elsewhere (Quinn[10]), rapid mixing in the near field. Sforza et al.[15] have named the nonlinear decay region the characteristic decay region because it depends on the shape and aspect ratio of a slot or nozzle. The decay in the linear decay region is more or less that of an axisymmetric jet. This is borne out by fitting the data in the linear decay region, by linear regression, to

$$\frac{U_{\max}}{U_{cl}} = K_u\left(\frac{X}{D_e} + C_u\right) \tag{1}$$

It is found that $K_u = 0.182$ and $C_u = 0.456$ in the range $28.67 \leq X/D_e \leq 62.58$. The mean streamwise velocity decay rate K_u of the present rectangular jet compares very well with that ($K_u = 0.183$) of an axisymmetric jet issuing from a sharp-edged slot.[11] The agreement between the three sets of data shown in Fig. 2 is good up to about $X/D_e = 10$. Further downstream, all three data sets show the same qualitative trends, but the quantitative agreement is rather poor. It should be recalled that damping screens surrounded the jet of the present study, whereas the use of such screens was not reported in the studies of Sforza et al.[15] and Sfeir.[2] The absence of such damping screens causes external disturbances, in the form of room draughts generated by the jet itself, to adversely affect both the mean streamwise velocity centerline decay and the spreading rates of the jet as has been shown by Bradshaw.[16]

Mean streamwise velocity contour plots at four streamwise locations are presented in Fig. 3. The dimensions on the plot boundaries in this figure, and in all subsequent figures involving contour maps, are in inches. The data for all of the contour maps were obtained on a grid at each streamwise measurement station. The grid spacing, which was kept constant at a given measurement station, was varied from 2.54 mm at $X/D_e = 2$ to 12.5 mm at $X/D_e = 20$. The estimated uncertainty in the measurement of the mean streamwise velocity is ±1% at 20:1 odds. The odds in all uncertainties

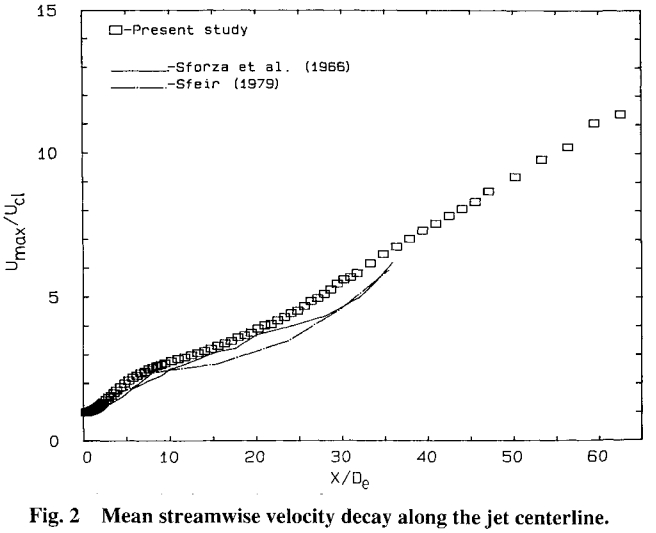

Fig. 2 Mean streamwise velocity decay along the jet centerline.

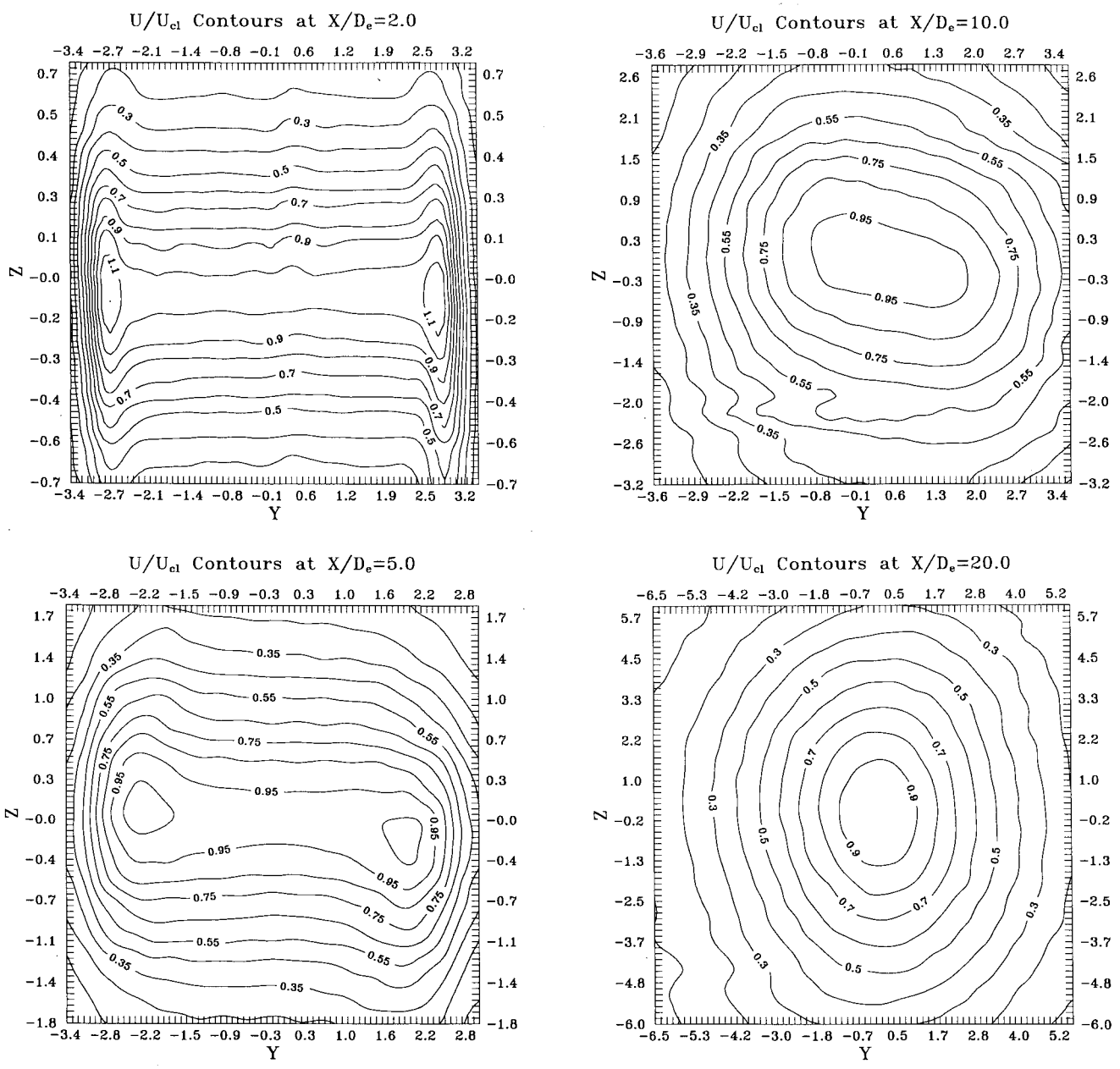

Fig. 3 Mean streamwise velocity contour plots; U/U_{cl}. All dimensions on the plot boundaries are in inches.

given subsequently will be the same (i.e., 20:1) and will, therefore, not be restated.

Mean streamwise velocity off-center peaks, which have also been observed by others,[1–10,15] are clearly visible at $X/D_e = 2$ and 5, and an effect of these, namely, the bulging of the contours at the corners, is present at $X/D_e = 2$ in Fig. 3. The mean streamwise velocity off-center peaks will be discussed further in connection with the mean streamwise vorticity contour maps. The jet, as judged by the position of the 0.5 contour line, grows monotonically in the Z direction but contracts in the Y direction up to about $X/D_e = 10$. The jet shape changes from rectangular at $X/D_e = 2$ to elliptical at $X/D_e = 20$. According to Bradshaw,[17] this change in shape of the mean streamwise velocity field is due to turbulence-generated secondary flows (Prandtl's secondary flows of the second kind). Since the contribution of the anisotropy of the Reynolds normal stresses to the generation of secondary flows is small in free flows and the Reynolds secondary shear stress ($\overline{v'w'}$), which plays an important role in turbulence-generated secondary flows, was not measured, another vehicle for explaining the change in shape of the jet must be sought. The unstable nature of the issuing of the jet of air from the rectangular slot into ambient air will trigger the production of vortex rings in the shear layers outside the jet core.[18] Such vortex rings will necessarily have the rectangular shape prescribed by the slot initially. Now, as is well known,[19] the curvature variation of a vortical structure, such as a vortex ring, in the circumferential direction results in the nonuniform self-induction and hence the deformation of the vortical structure. This accounts for the observed change in shape of the jet as depicted in Fig. 3. One effect of the deformation of the surrounding vortex ring, brought about by the fact that the corners will move faster than other points on the vortex ring, is what appears to be a rotation of the jet. This has been noted by Hussain and Husain[20] and observed in a triangular jet by Quinn.[21] It is clear that neither a triangular jet nor its rectangular counterpart actually rotates in bulk about its streamwise axis.

The secondary flow velocity vectors (i.e., the vector sums of the V and W velocities) are shown in Fig. 4. Abramovich[22] has hypothesized that a rectangular vortex ring will deform as a result of pressure imbalance between the long and short sides of the ring, with the pressure on the long sides, which are closer to the major axis of the vortex ring, being lower than the pressure on the short sides, which are farther away from the vortex ring minor axis. The pressure imbalance pumps flow from the short sides of the jet to the long sides in the plane of the jet cross section. This results in V velocities that are directed toward the center of the jet (i.e., in-

ward) and in W velocities that are directed away from the center of the jet (i.e., outward). It is reasonable to suppose diagonal symmetry in the case of the V velocities; of course, it is clear, bearing in mind the coordinate system defined in Fig. 1, that the V velocities below the diagonal will be negative and those above the diagonal will be positive. Diagonal symmetry of the secondary flow velocity vectors is clearly visible at $X/D_e = 5$ in Fig. 4. Two vortices are also observed: one in the upper right-hand corner and one in the lower left-hand corner of the flowfield at this location. Pollard and Schwab[8] have also found these vortices in the flowfield of a rectangular jet of aspect ratio 10. It is also clear that the W velocities in the upper half of the jet will be positive and that those in the lower half of the jet will be negative. The estimated uncertainty in the measurement of the mean spanwise and mean lateral velocities is ±3%.

The mean streamwise vorticity has been calculated from the V and W data, and the resulting mean streamwise vorticity contour plots are shown in Fig. 5. Note that positive and negative Ω_x indicate counterclockwise and clockwise rotation, respectively. Considering the flow through the three-dimensional contraction, which

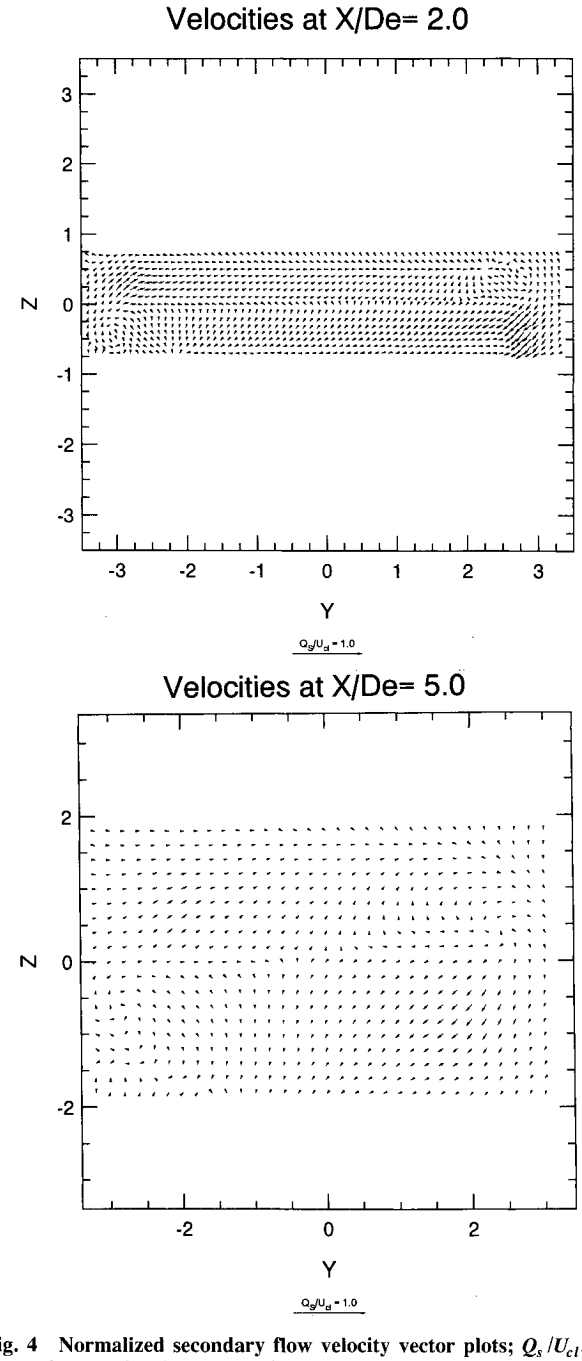

Fig. 4 Normalized secondary flow velocity vector plots; Q_s/U_{cl}. All dimensions on the plot boundaries are in inches.

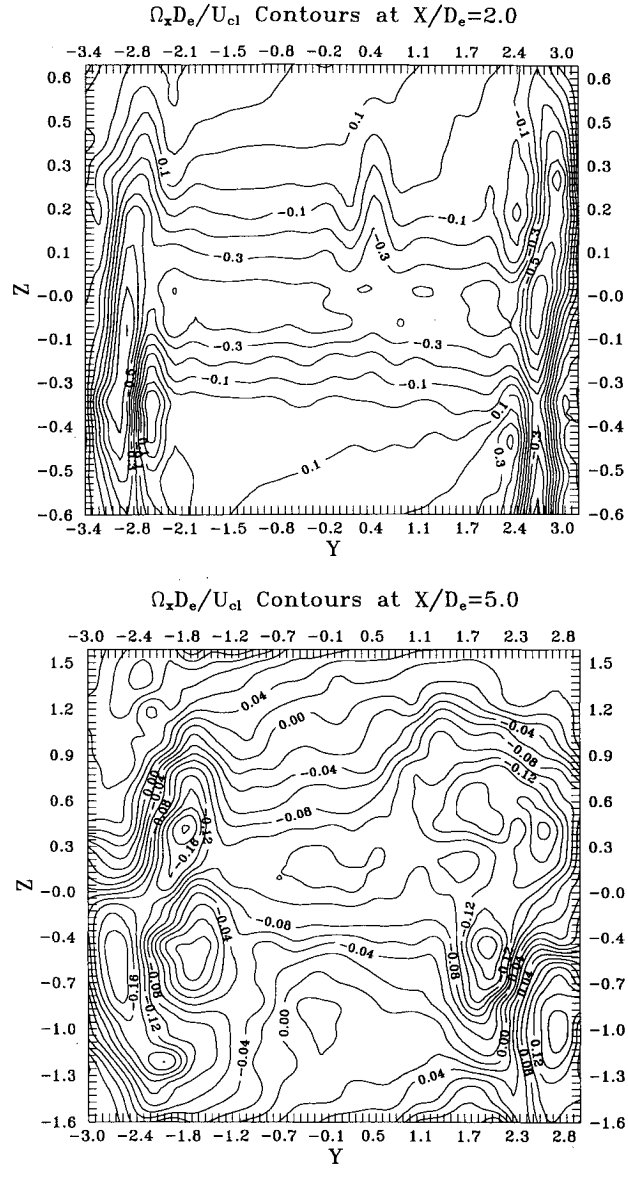

Fig. 5 Mean streamwise vorticity contour plots; $\Omega_x D_e/U_{cl}$. All dimensions on the plot boundaries are in inches.

is square in cross section, and applying the transport equation for the mean streamwise vorticity[17]:

$$U\frac{\partial \Omega_x}{\partial X} + V\frac{\partial \Omega_x}{\partial Y} + W\frac{\partial \Omega_x}{\partial Z} = \Omega_x\frac{\partial U}{\partial X} + \Omega_y\frac{\partial U}{\partial Y} + \Omega_z\frac{\partial U}{\partial Z}$$

$$+\left(\frac{\partial^2}{\partial Y^2} - \frac{\partial^2}{\partial Z^2}\right)(-\overline{v'w'}) + \frac{\partial^2}{\partial Y \partial Z}(\overline{v'^2} - \overline{w'^2})$$

$$+\left(\frac{\partial}{\partial X}\left(\frac{\partial \overline{u'v'}}{\partial Z} - \frac{\partial \overline{u'w'}}{\partial Y}\right) + \nu\nabla^2\Omega_x\right) \qquad (2)$$

it is found that mean streamwise vorticity is produced by the stretching of streamwise vortex lines brought about by the streamwise mean shear ($\partial U/\partial X$). Mean streamwise vorticity is also produced from the rotation for spanwise and lateral vortex lines in the X-Y and X-Z planes by the spanwise ($\partial U/\partial Y$) and lateral mean shear ($\partial U/\partial Z$), respectively, and, to a lesser extent, from gradients in the Reynolds spanwise and lateral normal stresses and the secondary shear stress. The mean streamwise vorticity thus produced is convected downstream in the three-dimensional contraction. As the flow leaves the slot exit plane, the vortices must necessarily

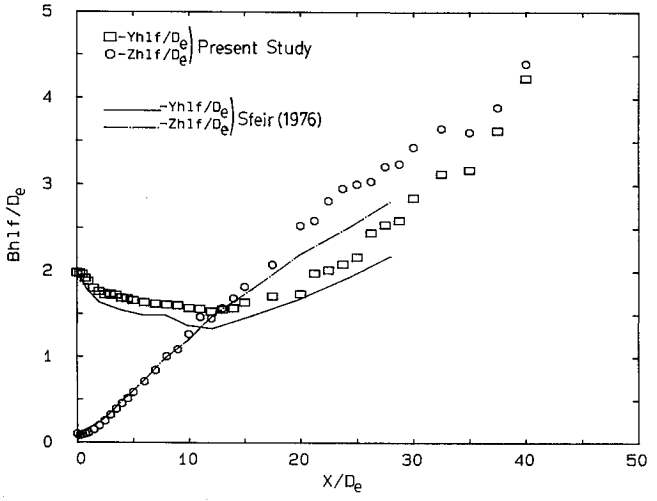

Fig. 6 Jet half-velocity width growth.

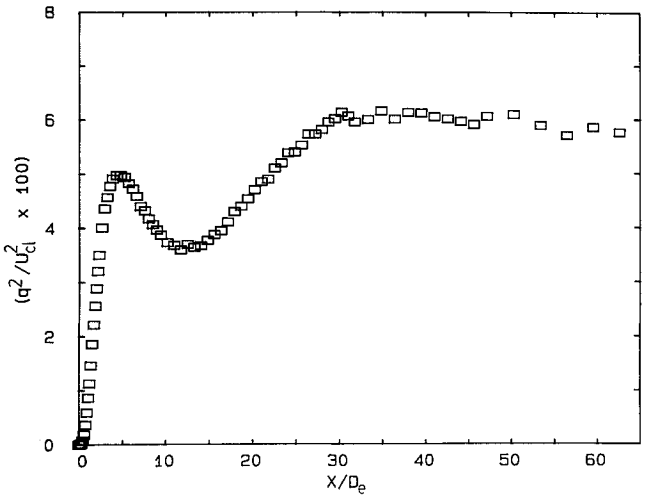

Fig. 7 Variation of the turbulence kinetic energy along the jet centerline.

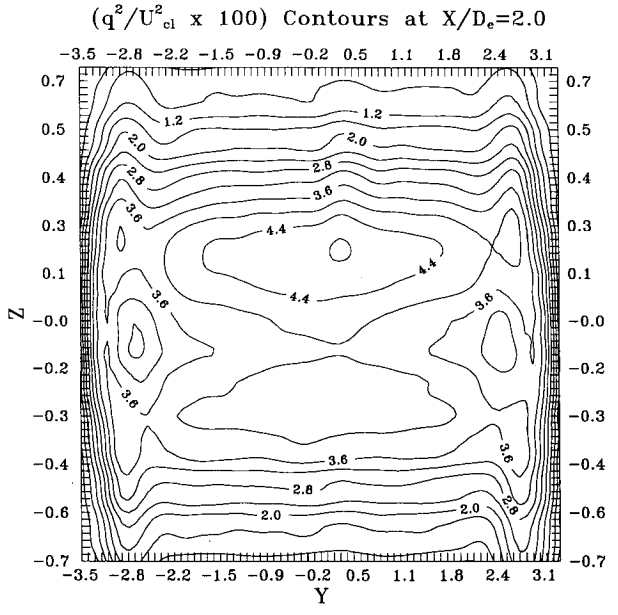

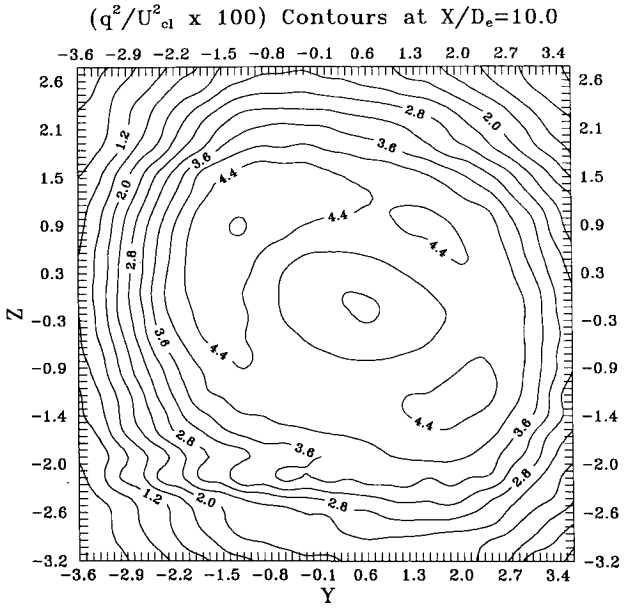

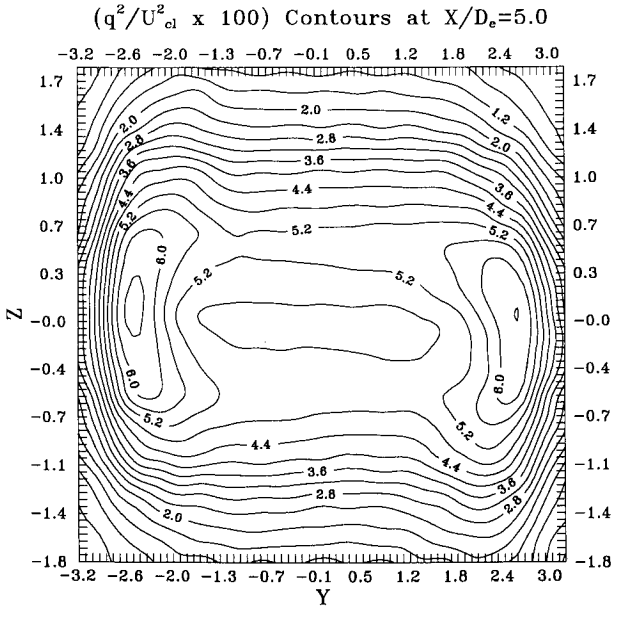

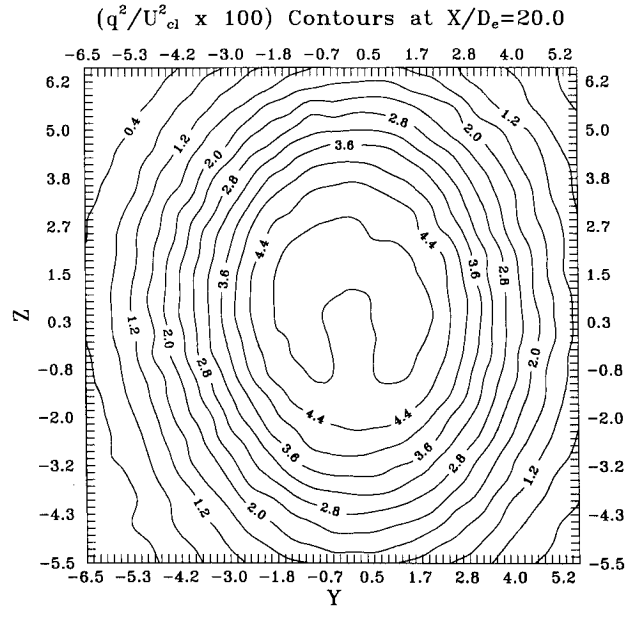

Fig. 8 Turbulence kinetic energy contour plots; $q^2/U_{cl}^2 \times 100$. All dimensions on the plot boundaries are in inches.

exist as counter-rotating pairs, as Fig. 5 shows, since vorticity cannot be created within the core of a homogeneous fluid.[19] The observed mean streamwise velocity off-center peaks may be the result of the self-induction of the counter-rotating streamwise vortices. The counter-rotating streamwise vortices will also facilitate rapid mixing by acting as vehicles for moving high-momentum fluid to areas where there is low-momentum fluid and vice versa. The estimated uncertainty in the mean streamwise vorticity is ±19.5%.

The growth of the jet half-velocity width in the two central planes of symmetry is shown in Fig. 6 along with the results of Sfeir.[1] The half-velocity width is the distance from the streamwise axis of a point, in the flowfield, where the mean streamwise velocity is half its value on the streamwise axis. The *Zhlf* grows monotonically, whereas *Yhlf* decreases initially. The *Zhlf* and *Yhlf* have the same value at about $X/D_e = 13$ after which *Yhlf* exceeds *Zhlf* in the far flowfield. The behavior of both half-velocity widths is consistent with the previously described deformation of the rectangular jet cross section based on the Abramovich hypothesis. The use of damping screens was not reported by Sfeir[1]; the absence of such damping screens may have caused external disturbances, as mentioned previously, to adversely affect the half-velocity width growth of the jet[16] and thus accounts for the lack of agreement between the two sets of data beyond $X/D_e = 10$.

The variation of the turbulence kinetic energy along the jet centerline is shown in Fig. 7. It should be noted that all three of the Reynolds normal stresses were measured. The steep rise in the turbulence kinetic energy in the very near flowfield is due to the growth and interaction, with the concomitant high turbulent activity, of the shear layers emanating from all four sides of the slot. It is clear that the turbulence kinetic energy, which is produced in the shear layers, is transported by diffusion and convection to the jet centerline; hence the peak in the turbulence kinetic energy distribution signals the arrival of the shear-layer structures at the jet centerline. The pronounced centerline turbulence kinetic energy peak observed in the present flow has been attributed by Hill et al.[23] to laminar initial nozzle boundary layers. One should then expect to find pronounced centerline turbulence kinetic energy peaks in all jet flows with laminar exit-plane flow. This, however, is not the case. Indeed, as the study of Quinn[10] has shown, such peaks are not observed in jet flows issuing from rectangular slots of aspect ratio less than 5 and from circular slots even though the exit-plane flows were laminar. Browne et al.[24] have shown that a pronounced turbulence kinetic energy peak on the jet centerline is more likely

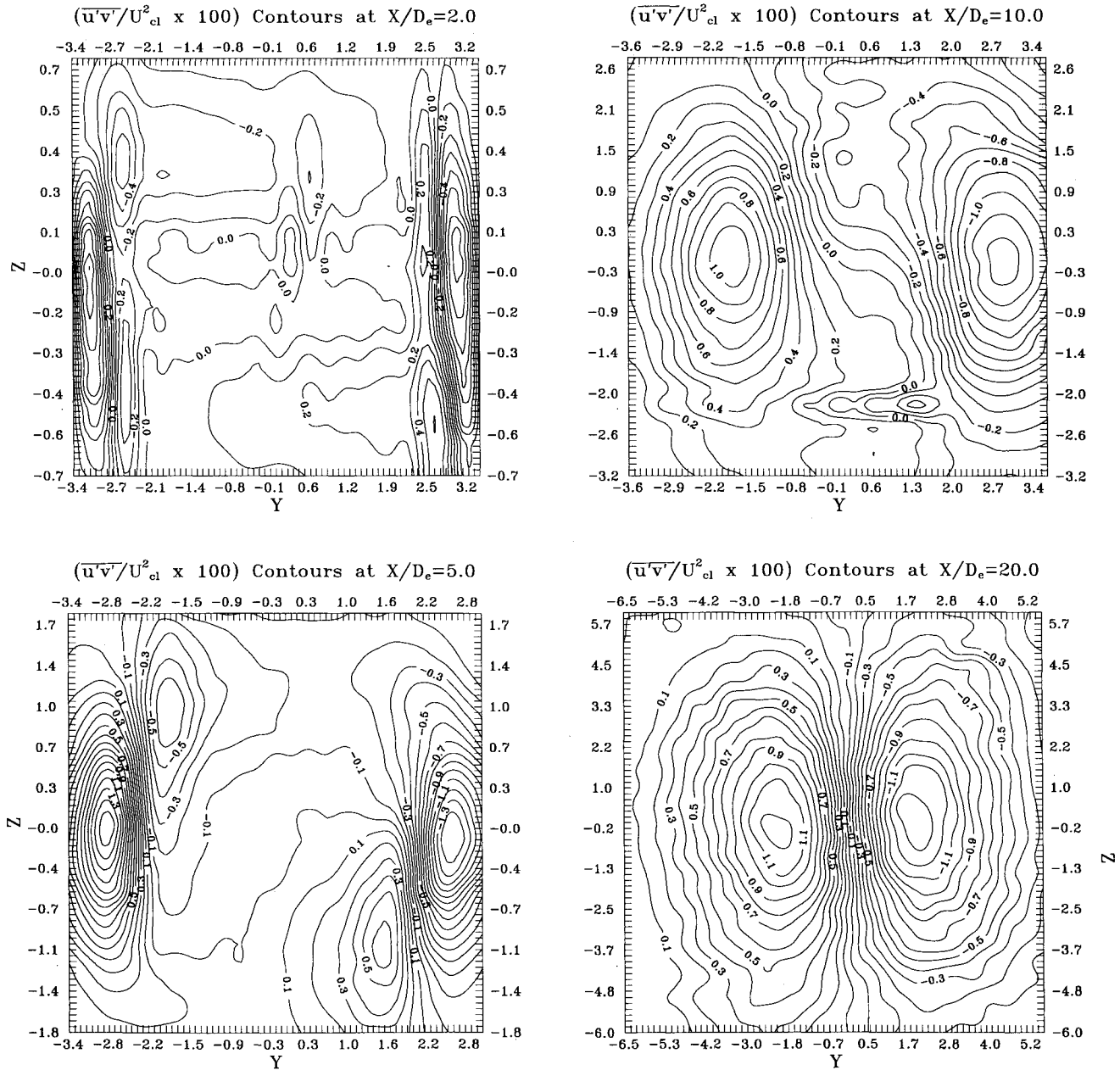

Fig. 9 Spanwise Reynolds primary shear stress contour plots; $\overline{u'v'}/U_{cl}^2 \times 100$. All dimensions on the plot boundaries are in inches.

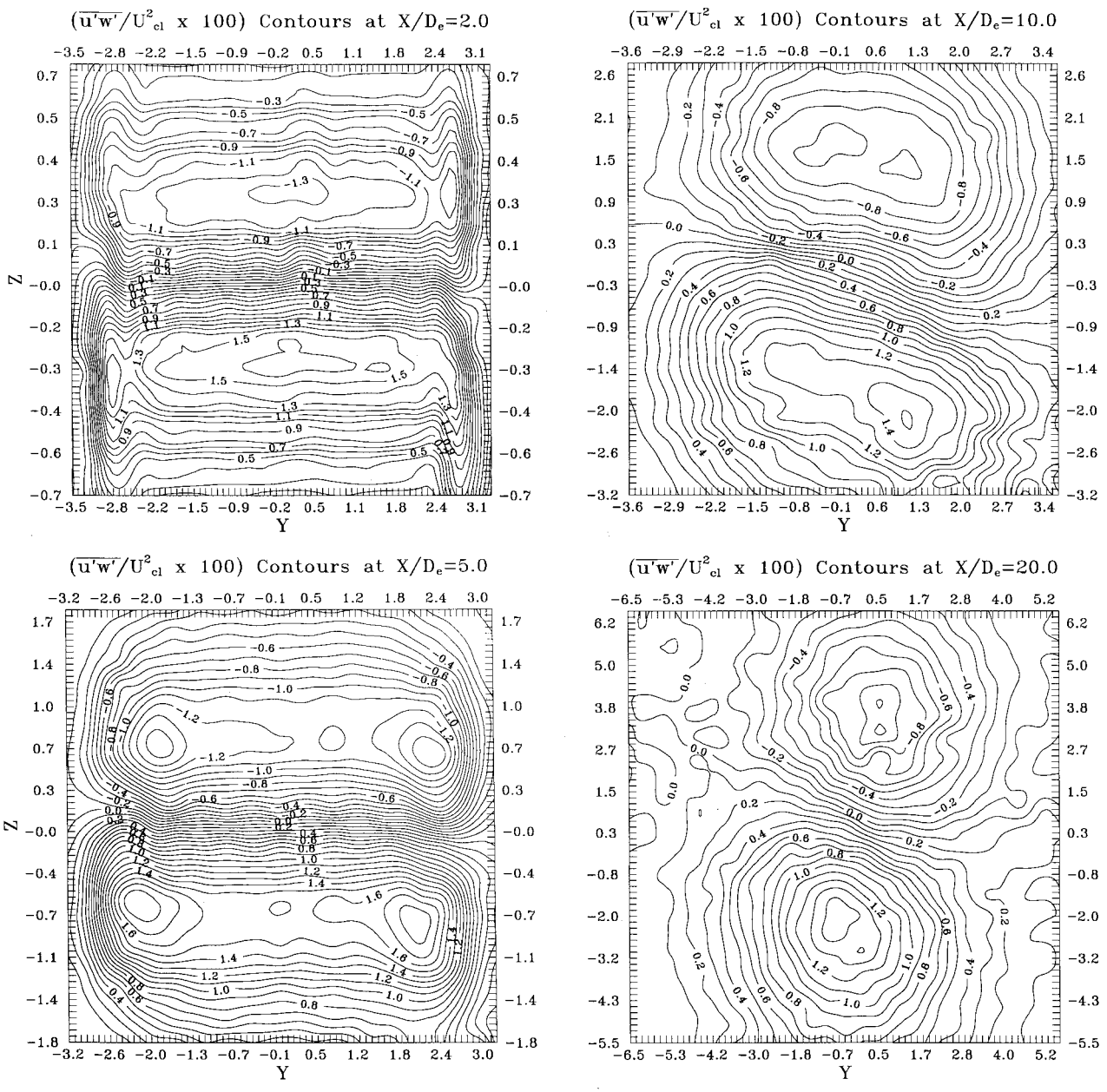

Fig. 10 Lateral Reynolds primary shear stress contour plots; $\overline{u'w'}/U_{cl}^2 \times 100$. All dimensions on the plot boundaries are in inches.

to be found in jet flows with symmetric, relative to the jet centerline, shear-layer structures. The present jet flow can be considered to be approximately self-preserving, as Fig. 7 shows, beyond $X/D_e = 30$.

Turbulence kinetic energy contour plots are shown in Fig. 8. The turbulence kinetic energy was calculated from the measured Reynolds normal stresses. The shapes of the turbulence kinetic energy contours are similar to those of the mean streamwise velocity contours shown in Fig. 3 at the corresponding streamwise locations. The spanwise and lateral local shear in the mean streamwise velocity have been calculated, and contour maps of these quantities have been obtained; however, for space reasons these contour maps are not presented here. It is clear, from the available evidence, that both the spanwise and lateral local shear in the mean streamwise velocity make the dominant contribution to the production of the turbulence kinetic energy. The turbulence kinetic energy contours exhibit good diagonal symmetry at $X/D_e = 2$ and beyond. It should be mentioned, as stated previously, that the diagonal symmetry is a consequence of the deformation of the jet cross section. The maximum values of the turbulence kinetic energy in the very near region ($X/D_e \leq 5$) of the jet are much higher than those found in the same region of a round jet[25] and of lower-aspect-ratio rectangular jets,[10] which is an indication of enhanced mixing. The estimated uncertainty in the turbulence kinetic energy data is ±5.2%.

The spanwise and lateral Reynolds primary shear stress contour plots are shown in Figs. 9 and 10, respectively. The spanwise local shear in the mean streamwise velocity in the central part of the jet at $X/D_e = 2$ is zero since the spanwise shear layers (i.e., those emanating from the short sides of the slot) are still developing. The spanwise Reynolds primary shear stress is, therefore, very small at this station (see Fig. 9). Note that the spanwise Reynolds primary shear stress values in Fig. 9 must be divided by 100. The maximum values of the lateral Reynolds primary shear stress (see Fig. 10) are larger than those of the spanwise Reynolds primary shear stress (see Fig. 9) in the very near flowfield (i.e., $X/D_e \leq 5$). The lateral shear layers are indeed fully developed, whereas the spanwise shear layers are still developing in this region as has already been mentioned. In general, there is a close correspondence between the spanwise local shear in the mean streamwise velocity and the spanwise Reynolds primary shear stress and between the lateral local shear in the mean streamwise velocity and the lateral Reynolds primary shear stress. This may imply that the principal axes of the Reynolds primary shear stresses and the corresponding

strains are coaligned and thus suggest that a Boussinesq-type, eddy-viscosity turbulence model may be appropriate to calculate the present flow. However, caution must be exercised since it is known[10] that there are small regions of negative production of turbulence kinetic energy in the flow. The local shear in the mean streamwise velocity and the corresponding Reynolds primary shear stress have opposite signs and a Boussinesq-type, eddy-viscosity turbulence model will fail to calculate correctly the Reynolds primary shear stresses in such regions. The Reynolds primary shear stresses in the near flowfield of the present flow are larger than those found in a round turbulent free jet[25] and in lower-aspect-ratio rectangular turbulent free jets[10] at the corresponding locations. This provides further evidence of enhanced mixing in the present flow. The estimated uncertainty in the measurement of the spanwise and lateral Reynolds primary shear stresses is ±8%.

Conclusions

Detailed measurements of the mean velocity components and the Reynolds normal and primary shear stresses have been made, using hot-wire anemometry, in the flowfield of an incompressible, turbulent free air jet issuing into still air surroundings from a sharp-edged rectangular slot of aspect ratio 20. Such a detailed data set for this slot aspect ratio has been unavailable until now.

It was found, first, that the near flowfield of the jet is dominated by counter-rotating pairs of streamwise vortices (Prandtl's secondary motion of the first kind), which facilitate enhanced mixing of the jet by acting as vehicles of transfer of high-momentum fluid to areas of low-momentum fluid and vice versa. Second, the mean streamwise velocity off-center peaks, which may be the result of the self-induction of the counter-rotating streamwise vortices, exist in the near flowfield of the jet. Third, the jet changes its shape from rectangular initially to elliptical in the far flowfield, and this change in shape is brought about by the deformation of the circumferential rectangular vortex rings (shed at the slot exit plane) as a result of nonuniform self-induction. Fourth, the flow is directed from the short to the long sides of the jet and thus accounts for the rapid initial growth of the jet in the lateral direction and its initial contraction in the spanwise direction. Fifth, the turbulence kinetic energy (derived from the Reynolds normal stress measurements) and Reynolds primary shear stress values in the very near flowfield of the jet are higher than those found in a round turbulent free jet and in lower-aspect-ratio rectangular free jets thus providing further evidence, in addition to a very short potential core, of enhanced near-field mixing of the present flow. Finally, the turbulence kinetic energy and Reynolds primary shear stress fields correspond closely to the local shear in the mean streamwise velocity field.

Acknowledgment

This work was supported by a grant from the Natural Sciences and Engineering Research Council of Canada.

References

[1]Sfeir, A. A., "The Velocity and Temperature Fields of Rectangular Jets," *International Journal of Heat and Mass Transfer*, Vol. 19, No. 12, 1976, pp. 1289–1297.

[2]Sfeir, A. A., "Investigation of Three-Dimensional Rectangular Jets," *AIAA Journal*, Vol. 17, No. 10, 1979, pp. 1055–1060.

[3]Marsters, G. F., "The Effects of Upstream Nozzle Shaping on Incompressible Turbulent Flows from Rectangular Nozzles," *Transaction of the Canadian Society for Mechanical Engineering*, Vol. 5, No. 4, 1979, pp. 197–203.

[4]Marsters, G. F., "Spanwise Velocity Distributions in Jets from Rectangular Slots," *AIAA Journal*, Vol. 19, No. 2, 1981, pp. 148–152.

[5]Marsters, G. F., and Fotheringham, J., "The Influence of Aspect Ratio on Incompressible, Turbulent Flows from Rectangular Slots," *The Aeronautical Quarterly*, Vol. 31, Pt. 4, 1980, pp. 285–305.

[6]Quinn, W. R., Pollard, A., and Marsters, G. F., "Measurements in a Turbulent Rectangular Free Jet," *Proceedings of the 4th Symposium on Turbulent Shear Flows* (Univ. of Karlsruhe, Karlsruhe, Germany), Sept. 1983, pp. 7.1–7.6.

[7]Tsuchiya, Y., Horikoshi, C., and Sato, T., "On the Spread of Rectangular Jets," *Experiments in Fluids*, Vol. 4, No. 4, 1986, pp. 197–204.

[8]Pollard, A., and Schwab, R. R., "The Near-Field Behavior of Rectangular Free Jets: An Experimental and Numerical Study," *Proceedings of the 1st World Conference on Experimental Heat Transfer, Fluid Mechanics and Thermodynamics*, Elsevier, New York, 1988, pp. 1510–1517.

[9]Quinn, W. R., "Passive Near-Field Mixing Enhancement in Rectangular Jet Flows," *AIAA Journal*, Vol. 29, No. 4, 1991, pp. 515–519.

[10]Quinn, W. R., "Turbulent Free Jet Flows Issuing from Sharp-Edged Rectangular Slots: The Influence of Slot Aspect Ratio," *Experimental Thermal Fluid Science*, Vol. 5, No. 2, 1992, pp. 203–215.

[11]Quinn, W. R., and Militzer, J., "Experimental and Numerical Study of a Turbulent Free Square Jet," *Physics of Fluids*, Vol. 31, No. 5, 1988, pp. 1017–1025.

[12]Bradshaw, P., *An Introduction to Turbulence and Its Measurement*, Pergamon, Oxford, England, UK, 1975.

[13]Bearman, P. W., "Corrections for the Effect of Ambient Temperature Drift on Hot-Wire Measurements in Incompressible Flow," *DISA Information*, Vol 11, No. 11, 1971, pp. 25–30.

[14]Champagne, F. H., and Sleicher, C. A., "Turbulence Measurements with Inclined Hot-Wire Probes—Pt. 2: Hot-Wire Response Equations," *Journal of Fluid Mechanics*, Vol. 28, Pt. 1, 1967, pp. 177–182.

[15]Sforza, P. M., Steiger, M. H., and Trentacoste, N., "Studies on Three-Dimensional Viscous Jets," *AIAA Journal*, Vol. 4, No. 5, 1966, pp. 800–806.

[16]Bradshaw, P., "Effect of External Disturbances on the Spreading Rate of a Plane Turbulent Jet," *Journal of Fluid Mechanics*, Vol. 80, Pt. IV, 1977, pp. 795–797.

[17]Bradshaw, P., "Turbulent Secondary Flows," *Annual Review of Fluid Mechanics*, Vol. 19, 1987, pp. 53–74.

[18]Vallentine, H. R., *Applied Hydrodynamics*, Plenum, New York, 1967.

[19]Batchelor, G. K., *An Introduction to Fluid Mechanics*, Cambridge Univ. Press, Cambridge, England, UK, 1967.

[20]Hussain, F., and Husain, H. S., "Elliptic Jets, Part 1: Characteristics of Unexcited and Excited Jets," *Journal of Fluid Mechanics*, Vol. 208, Nov. 1989, pp. 257–320.

[21]Quinn, W. R., "Mean Flow and Turbulence Measurements in a Triangular Turbulent Free Jet," *International Journal of Heat and Fluid Flow*, Vol. 11, No. 3, 1990, pp. 220–224.

[22]Abramovich, G. N., "On the Deformation of the Rectangular Turbulent Jet Cross-Section," *International Journal of Heat and Mass Transfer*, Vol. 25, No. 18, 1982, pp. 1885–1894.

[23]Hill, W. G., Jenkins, R. C., and Gilbert, B. L., "Effects of the Initial Boundary Layer State on Turbulent Jet Mixing," *AIAA Journal*, Vol. 14, No. 11, 1976, pp. 1513,1514.

[24]Browne, L. W. B., Antonia, R. A., and Chambers, A. J., "The Interaction Region of a Turbulent Plane Jet," *Journal of Fluid Mechanics*, Vol. 149, Dec. 1984, pp. 355–373.

[25]Boguslawski, L., and Popiel, C. O., "Flow Structure of the Free Round Turbulent Jet in the Initial Region," *Journal of Fluid Mechanics*, Vol. 90, Pt. III, 1979, pp. 531–539.